Self-Organized Stationary States of Tokamaks

S. C. Jardin, N. Ferraro, and I. Krebs

Phys. Rev. Lett. **115**, 215001 — Published 17 November 2015

DOI: 10.1103/PhysRevLett.115.215001

Self-organized Stationary States of Tokamaks

S.C. Jardin,[1] N. Ferraro,[2] and I. Krebs[1,3]

[1] *Princeton Plasma Physics Laboratory, P.O.Box 451, Princeton, NJ 08543 USA*
[2] *General Atomics, P.O. Box 85608, San Diego, CA 92186 USA*
[3] *Max-Plank-Institut für Plasmaphysik, Garching, Germany*

(Dated: September 23, 2015)

We demonstrate that in a 3D resistive magnetohydrodynamic (MHD) simulation, for some parameters it is possible to form a stationary state in a tokamak where a saturated interchange mode in the center of the discharge drives a near helical flow pattern that acts to non-linearly sustain the configuration by adjusting the central loop voltage through a dynamo action. This could explain the physical mechanism for maintaining stationary non-sawtoothing "hybrid" discharges, often referred to as "flux-pumping".

PACS numbers: 52.30.Cv 52.55.Fa 52.65.kj

Typical high-performance modes of tokamak operation undergo "sawtooth" cycles, in which the peaking of the central current density triggers a periodic core instability which redistributes the current density. However, certain modes of operation are known, such as the "hybrid" mode in DIII-D [1] and other tokamaks [2–7], which do not experience this cycle of instability. Empirically, it is observed that these modes maintain a non-axisymmetric equilibrium which somehow limits the peaking of the toroidal current density. The physical mechanism responsible for this has not previously been understood, but has been referred to as "flux-pumping", in which poloidal flux is anomalously redistributed and the toroidal current broadened in order to maintain the central safety factor (ratio of times a given magnetic field line travels around the torus the long way to the short way) greater than unity, $q_0 > 1$ [1]. Here we show that in simulations of inductively driven tokamak plasmas, a steady-state non-axisymmetric magnetic equilibrium may be obtained in which $q_0 > 1$ is maintained by a nonlinear dynamo action driven by a stationary marginal core interchange mode.

An inductively driven tokamak plasma is said to be in a *stationary state* if the magnetic field, temperatures, and densities (and hence pressure) are not changing in time. If this state is achieved, it is normally reached late in the discharge after the plasma current is constant in time and has fully penetrated. Since the magnetic field is not changing in time, it follows from Maxwell's induction equation that the electric field is the gradient of a single valued potential plus a constant times the gradient of the toroidal angle:

$$\frac{\partial \mathbf{B}}{\partial t} = -\nabla \times \mathbf{E} = 0 \;\; \Rightarrow \;\; \mathbf{E} = -\nabla\Phi + \frac{V_L}{2\pi}\nabla\varphi. \qquad (1)$$

Here, $\mathbf{B}$ and $\mathbf{E}$ are the magnetic and electric fields, Φ is a single valued potential, (R, φ, Z) are the usual cylindrical coordinates, and V_L is a spatial constant that represents the voltage the long way around the torus, created by external induction coils. In the resistive MHD description of a plasma, the generalized Ohm's law, $\mathbf{E}+\mathbf{V}\times\mathbf{B} = \eta\mathbf{J}$, combined with Eq. (1), gives the condition:

$$-\mathbf{V}\times\mathbf{B} + \eta\mathbf{J} = -\nabla\Phi + \frac{V_L}{2\pi}\nabla\varphi. \qquad (2)$$

Here, η is the resistivivty, $\mathbf{V}$ is the fluid velocity, and $\mathbf{J} = \mu_0^{-1}\nabla\times\mathbf{B}$ is the plasma current density in the low frequency (MHD) limit. Two projections of the vector Eq. (2) are of particular interest. The toroidal projection is given by:

$$\hat{\varphi}\cdot[-\mathbf{V}\times\mathbf{B} + \nabla\Phi] = -\eta J_\varphi + \frac{V_L}{2\pi R}. \qquad (3)$$

Here, the toroidal current density is represented as $J_\varphi \equiv \hat{\varphi}\cdot\mathbf{J}$. If we take the inner product of Eq. (2) with the magnetic field vector $\mathbf{B}$ we obtain:

$$\eta\mathbf{J}\cdot\mathbf{B} = -\mathbf{B}\cdot\nabla\Phi + \frac{V_L}{2\pi}\mathbf{B}\cdot\nabla\varphi. \qquad (4)$$

If magnetic surfaces exist everywhere, we can perform a surface average of Eq. (4) to obtain the well-known condition for tokamak stationary states:

$$\frac{\langle\mathbf{J}\cdot\mathbf{B}\rangle}{\langle\mathbf{B}\cdot\nabla\varphi\rangle} = \frac{V_L}{2\pi\eta}. \qquad (5)$$

Here, $\langle\ \rangle$ is the standard surface average operator that annihilates $\mathbf{B}\cdot\nabla$ [8]. The plasma resistivity is a strong function of the plasma temperature: $\eta = \eta_0\, T^{-3/2}$ which is constant on the magnetic surfaces. From Eq. (5) we see that where the temperature is largest (typically in the center of the discharge due to central heating and geometrical effects) the surface averaged parallel current density will also be largest. This large current will lead to a large Ohmic heating term in the temperature equation which tends to increase the central temperature even more, thus requiring the plasma current to peak even more in order to satisfy Eq. (5) .

The conventional explanation [9] for why this thermal instability doesn't continue to peak the current to very

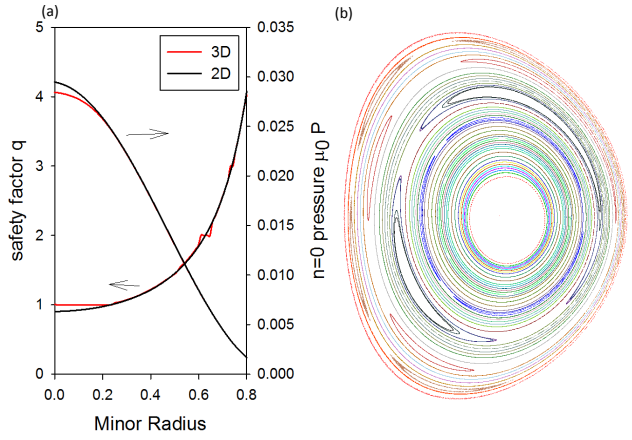

FIG. 1. (a) Comparison of q-profile and toroidally averaged pressure for stationary state 3D run and 2D run with exactly the same transport coefficients. (b)Poincaré plot of the magnetic field in the final state with $(2,1)$ and $(3,1)$ islands present. Center volume has $q = 1$.

large values is the "sawtooth" cycle. The safety factor at the plasma center is inversely proportional to the current density at the center: $q_0 \simeq 2B_T/\mu_0 J_0 R_0$, where B_T is the toroidal field strength and R_0 is the major radius. As the current continues to peak, eventually the central safety factor falls below unity and the configuration becomes unstable to an internal resistive-kink mode [10] with approximate angular dependence, $\cos(\theta - \varphi)$ where θ is the angle the short way around the torus (in the R, Z plane). We call this a $(m, n) = (1, 1)$ mode referring to the multipliers of the two angles. This causes a reconnection event to occur that tends to flatten both the current and the temperature profiles so that q_0 suddenly increases to above unity, and the process then repeats cyclically so that the configuration is not strictly stationary on all timescales.

We report here on a different mechanism for preventing the current and temperature profiles from peaking in a truly stationary state tokamak. For certain global parameters, regardless of the initial state, the plasma profiles will evolve into a self-organized state with the central safety factor slightly above unity and constant in a central volume. We illustrate such a configuration in Figure (1). The solid curves in Fig. (1a) show the steady state pressure and safety factor profiles along the outer major radius for a 3D simulation (red), and for an identical 2D (axisymmetric) calculation (black) with the same transport model and parameters. It is seen that the toroidally averaged 3D and 2D profiles differ in the center. Figure (1b) is a Poincaré plot of the final 3D magnetic configuration showing some island structure. The central shear-free region, omitted from the Poincaré plot, has $q \simeq 1$ and constant.

Such a large shear-free region with q just above unity is known to be linearly unstable to interchange modes driven by any non-zero pressure gradient [11–14]. Unlike an unstable configuration with a $q = 1$ resonant surface in the plasma, the unstable linear eigenfunction for a ultra-low shear configuration with q just above 1 throughout a volume is distributed out to the region where the shear begins (about the $q = 1.01$ surface) and the instability drives a strong $(1, 1)$ helical flow. The unstable linear eigenfunction found in [13] is given in terms of the velocity stream function U by:

$$U = U_0 r \left[1 - (r/r_1)^2\right] \sin(\theta - \varphi) . \qquad (6)$$

Here the minor radius is $r = |R - R_0|$ and r_1 is the minor radius where the shear becomes non-zero. The steady-state condition, Eq. (4), does not explicitly contain the velocity. However, the driven flow creates a $(1, 1)$ component of the electrostatic potential Φ and of the magnetic field $\mathbf{B}$ that combine to create a $(0, 0)$ spatially varying "dynamo" voltage that prevents the current density from peaking in the center and hence maintains q slightly above unity and shear-free in the central region. We note here that the role of the electrostatic potential in maintaining near-stationary single helicity states in the reversed field pinch has been emphasized previously [15].

The flow field also acts nonlinearly to partially flatten the temperature and hence resistivity profile in the center, thus reducing the tendency for the current to peak [16]. However, as will be shown in Figures (3) and (4), this effect is normally secondary to the generation of the spatially varying dynamo voltage. The self-consistent calculations presented here illustrating the formation of the dynamo voltage were performed with the M3D-C1 [17] toroidal 3D MHD code, and could possibly explain non-sawtoothing discharges with $q_0 \simeq 1$ such as hybrid modes in DIII-D [1], ASDEX-U [2], JT-60U [3] and JET [4, 5] , and long-lived modes in NSTX [6] and MAST [7]. Stationary non-sawtoothing behavior has been observed in other 3D tokamak MHD simulations [18–20] but an explanation of how these configurations maintain themselves over resistive timescales has not appeared.

The poloidal velocity in M3D-C1 is represented as $\mathbf{V} = R^2 \nabla U \times \nabla\varphi + R^{-2} \nabla_\perp \chi$, a form of a Hodge decomposition. Here $\nabla_\perp$ indicates the gradient perpendicular to the toroidal direction. In all the results presented here the kinetic energy in the χ field is less than 1% of the energy in the U field (which does not compress the strong toroidal magnetic field) and can thus be ignored in the analysis. Inserting this into Eq. (3) and rearranging:

$$-R\mathbf{B} \cdot \nabla U + \hat{\varphi} \cdot [F \nabla U + \nabla \Phi] = -\eta J_\varphi + \frac{V_L}{2\pi R}. \qquad (7)$$

We made use of the M3D-C1 form of the magnetic field:

$$\mathbf{B} = \nabla\psi \times \nabla\varphi - \nabla_\perp \partial f/\partial\varphi + F\nabla\varphi, \qquad (8)$$

and $F \equiv F_0 + \nabla_\perp^2 f$, with F_0 a constant. We find that the two terms in the bracket cancel to a high degree, $\nabla\Phi \simeq -F\nabla U$, so that Eq. (7) becomes:

$$\eta J_\varphi = R\mathbf{B}\cdot\nabla U + \frac{V_L}{2\pi R}. \qquad (9)$$

This is seen to be very similar in form to Eq. (4). Both Eq. (9) and Eq. (4) have a nonlinear term of the form $\mathbf{B}\cdot\nabla\Phi \simeq -F\mathbf{B}\cdot\nabla U$ as well as a nonlinear term in involving the resistivity η and the current density.

In the illustrative simulations presented here, we solve the single fluid 3D (or 2D) resistive MHD equations with source terms as described in [17]. To illustrate the self-organized voltage clamping mechanism, we present results from 5 long time simulations. We chose a tokamak plasma with a generic shape for the last closed flux surface: $R = R_0 + a\cos(\theta + \delta\sin\theta), Z = b\sin(\theta)$, with $R_0 = 3.2$ m, $a = 1.0$ m, $b = 1.3$ m, and $\delta = 0.2$. The toroidal field on axis was $B_0 = F/R_0 = 1$ T and the plasma current was $\mu_0 I_T = 0.8$ T m so that the edge safety factor was $q_{edge} \simeq 4.5$. The runs were largely identical with central resistivity in MKS units $\eta_0 = 10^{-6}(\mu_0/\tau_A)\,\mathrm{m}^2$, where, $\tau_A = a\sqrt{\mu_0\rho}/B_0$, and plasma beta: $\beta \equiv 2\mu_0\langle p\rangle/B_0^2 = 2\%$. The four fully 3D simulations differed in that a multiplier was applied to both the isotropic thermal conductivity and the heating sources so that they would balance and keep $\beta = 2\%$. The 4 values used were $\kappa_0 = C \times \eta_0/\mu_0$ with $C = 18, 36, 72, 144$. The thermal conductivity varied with the plasma temperature as $\kappa = \kappa_0(T/T_0)^{-1/2}$.

The calculations in this paper all have $\beta = 2\%$. The stationary behavior obtained is fundamentally different from that in simulations at lower values of β. In particular, we have performed a similar sequence of calculations with $\beta = 0.06$ and these all exhibit periodic sawteeth oscillations. The presence of a β threshold for the existance of stationary states is consistent with earlier computational studies [18].

A large constant parallel thermal conductivity of $\kappa_\parallel = (10/\tau_A)m^2$ was used in all simulations. A loop voltage was applied at the plasma boundary with a feedback loop to keep the total toroidal current constant in time, as is normally done in experiments. Each simulation was also run in a 2D (axisymmetric) mode in which all toroidal derivatives were set to zero, for comparison. The simulations were run to long times: $T = 10^5\tau_A$ such that everything became time-independent. A typical stationary self-organized state for the 3D $C = 144$ case is shown in Fig. (1)-(2). The right side of Fig. (2) shows contours of the M3D-C1 poloidal velocity stream function interior to the $q = 1.01$ surface at 4 toroidal angles, and the line plot on the left shows a comparison of the computed stream function and the linear unstable eigenfunction as given by Eq. (6) with $U_0 = 3.12\times10^2 m/s$ and $r_1 = 0.3m$.

Consider now Eq. (4). In Fig. (3) we show the difference of the mid-plane value of the toroidally averaged voltage drop along the magnetic field that is present in the four 3D runs from that in the corresponding 2D runs. This fundamentally 3D dynamo voltage is obtained by plotting the difference of the toroidally averaged first term on the right side of Eq. (4) for each of the four 3D runs from that in its corresponding 2D run:

$$\frac{B}{2\pi R}V_{dyn} = \frac{1}{2\pi}\int_0^{2\pi}[-\mathbf{B}\cdot\nabla\Phi]_{3D}\,d\varphi - [-\mathbf{B}\cdot\nabla\Phi]_{2D} \qquad (10)$$

Here, V_{dyn} is the axisymmetric ($n = 0$) voltage that is present in the 3D runs that is not present in the 2D run and is therefore due to the 3D dynamo effect driven by the interchange instability. This voltage is exactly that needed to reduce the central current density so as to keep q in the center just above 1 and shear-free as can be seen in the q-profiles for the four runs in Fig. (3b).

The required dynamo voltages for each of the four runs are different because of the differing temperature and

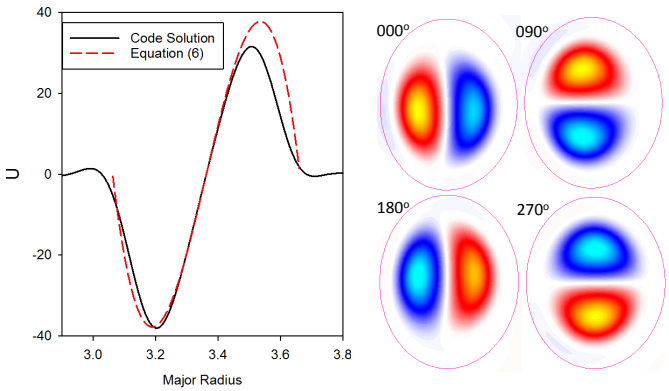

FIG. 2. Right shows contours of M3D-C1 velocity stream function U interior to the $q = 1.01$ surface at 4 toroidal angles. Curves on left compare midplane values at $\varphi = 180^0$ with linear eigenfunction found in [13] and given by Eq. (6).

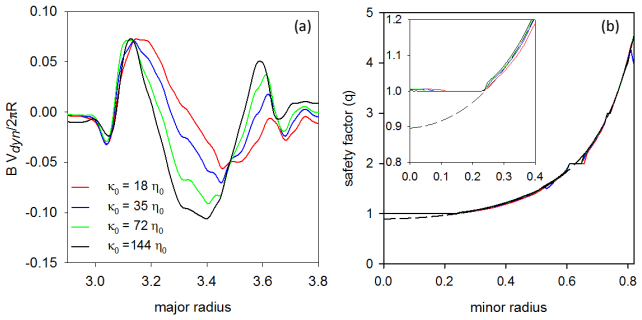

FIG. 3. (a) Effective mid-plane toroidal voltage increase in 4 different 3D stationary states over that in the equivalent 2D case. This voltage is due to dynamo action. (b) Final safety factor profile in the 4 3D runs (solid colors) and in the equivalent 2D runs (dashed).

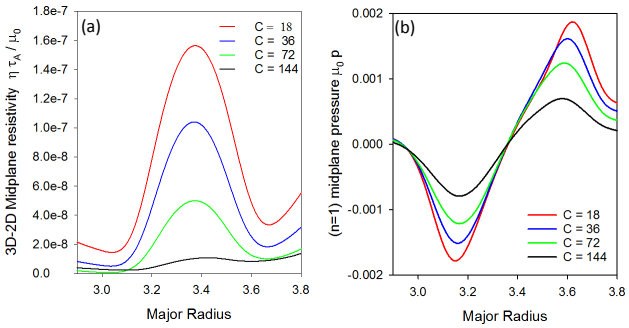

FIG. 4. Difference in the final (a) $n = 0$ midplane resistivity profiles and (b) midplane $n = 1$ pressure profile for each of the 4 cases from the equivalent 2D case.

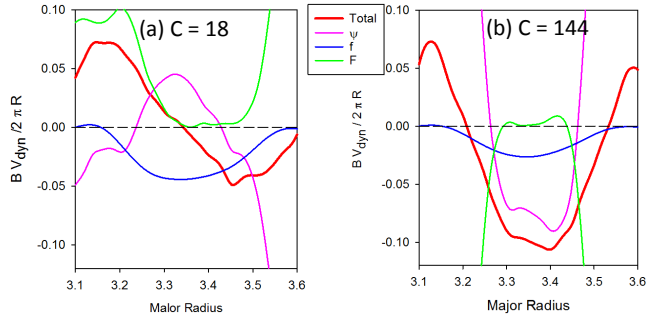

FIG. 5. Contribution to $[\mathbf{B}\cdot\nabla\Phi]_{n=0}$ for each of the field components on midplane interior to $q = 1.01$ surface.

hence resistivity flattening for the four runs as shown in Fig. (4a). The runs with the lowest thermal conductivity and energy source terms are most affected (flattened) by the interchange instability and so need the least dynamo voltage to maintain $q = 1$ in the center.

We next examine the 3 individual terms in $\mathbf{B}\cdot\nabla\Phi$ that correspond to the 3 magnetic field components in Eq. (8) for the two extreme cases to help clarify the mechanism that generates the dynamo voltage. As shown in Fig. (4b),the case with the smallest κ and source term, $C = 18$, develops the largest $(1,1)$ perturbation in the pressure, δp. From force balance, this perturbed pressure will cause a $(1,1)$ perturbation in the toroidal magnetic field function F in Eq. (8), $\delta F \simeq -\delta p \mu_0 R^2/F$. But this perturbed field component does not contribute to the toroidal average of $\mathbf{B}\cdot\nabla\Phi$ in the central region because δF is out of phase with $\partial\Phi/\partial\varphi$.

However, the poloidal component needed to keep the spatially varying toroidal field divergence free, i.e. the second term in Eq. (8), $-\nabla_\perp \partial f/\partial\varphi$, is in phase with $\nabla_\perp\Phi$ and thus does contribute to the dynamo voltage. The remaining term, $\nabla\psi\times\nabla\varphi\cdot\nabla\Phi$ is able to adjust to maintain the total dynamo voltage as required since the two perturbed fields ψ and Φ have the correct phase relation. To illustrate, we plot in Fig. (5) each of the 3 components of the axisymmetric ($n = 0$) component of $\mathbf{B}\cdot\nabla\Phi$ (minus its value in the companion 2D run) for the two extreme cases C=18 and C=144. This clearly illustrates that there is a self-organized "feedback" mechanism involving the $(1,1)$ component of both the poloidal flux function ψ and the electrical potential Φ maintaining this stationary state.

Other theories for the sustainment of the hybrid discharges have appeared involving ad hoc hyper-resistivity [24], a rotating island driving current thru drift effects [25], and postulating a critical condition involving the poloidal current density [26]. However, none of these has been demonstrated to be self-consistent by way of a comprehensive three-dimensional time-dependent simulation as is done here.

Several experimental papers on hybrid discharges have appeared along with analysis that confirms that 2D evolution codes such as TRANSP or ASTRA would predict that the central safety factor with measured T_e profiles should fall to 0.8 or below whereas in reality it stays at 1.0. These sawtooth-free discharges have been correlated with a 3/2 tearing mode interacting with ELMs [1] and alternatively with the presence of fishbone modes [2, 27, 28]. However, a theory for how these MHD modes maintain the current profile has previously been lacking. In fact, it is stated in [1] "..we offer no conjecture as to how the coupling between the ELM and $m/n = 3/2$ NTM can broaden the current profile density...". Here we are suggesting that the nonlinear $(1,1)$ dynamo mechanism is responsible for maintaining the broad current profile, and that the tearing modes and fishbones are possibly a consequence of having a stationary $(1,1)$ mode with an ultraflat q-profile. The experimental observation [29] that on DIII-D a $n > 1$ tearing mode, usually a 3/2, is a necessary ingredient of the hybrid discharge is not fully explained in this paper, but it may be a bi-product of the $(1,1)$ mode by way of mode coupling as seen in Figure (1).

Similar MHD dynamos as discussed here have been shown to play a role in laminar RFP regimes, although with higher toroidal mode number n [15, 21]. It has also been recognized that dynamo-type effects could occur in tokamaks [see Eq. (40) of [22]], and helical core equilibrium states in tokamaks have been found in 3D equilibrium calculations [23] but the $(1,1)$ nonlinear dynamo mechanism for sustaining these equilibrium on a long (resistive) timescale as described in this paper has not previously been explicitly called out. Future studies will be concerned with better identifying which parameter regimes this is expected to occur when diamagnetic terms are present, what is the effect of sheared rotation, what is the role of the $(2,1)$ and possibly other islands such as the $(3,2)$ in supplying the dynamo voltage, and in making closer identification to experimental results, particularly in NSTX, DIII-D and ASDEX-U.

This work was supported by the U.S. DoE Award No.

DE-AC02-09CH11466, the Max-Plank Princeton Center for Plasma Physics, and the SciDAC Center for Extended MHD Modeling. The authors acknowledge useful discussions with A. Bhattacharjee, J. Breslau, J. Callen, G. Fu, S. Günter, S. Hudson, D. Meshcheriakov, R. Nazikian, C. Petty, and C. Sovinec, and essential software support from J. Chen and the SCOREC team at RPI.

[1] Petty, C., Austin, M.E., Holcomb, C. T. *et al.*, Phys. Rev. Lett. **102**, 045005 (2009)
[2] Sips, A.,Arslanbekov, R., Atanasiu, C. *et al.*, Plasma Phys. Control. Fusion **44**, B69 (2002)
[3] Oyama, N., Isayama, A., Matsunaga, G.*et al.*, Nucl. Fusion **49**, 065026 (2009)
[4] Joffrin, E., Crisanti, F.,Felton, R.*et al.*, Plasma Phys. Control. Fusion **45**, A367-A383 (2003)
[5] Buratti, P., Alper, B., Annibaldi, S.*et al.*, Plasma Phys. Control. Fusion **48**, 1005 (2006)
[6] Menard, J., Bell, R., Gates, D.*et al.*, Phys. Rev. Lett. **97**, 095002 (2006)
[7] Chapman, I., Hua, M., Pinches, S.D.*et al.*, Nucl. Fusion **50**, 045007(2010)
[8] Hinton, F. L.and Hazeltine, R. D., Rev. Mod. Phys. **48**, p. 239 (1976)
[9] Kadomtsev, B., Fiz. Plazmy 1 710 [Sov. J. Plasma Phys. **1**, 389 (1975):51]
[10] Ara, G., Basu, B., Coppi, B. *et al.*, Annals of Physics **112**, 443-476 (1978)
[11] Wesson, J., Plasma Phys. Control. Fusion **28**, 243 (1986)
[12] Hastie, R. J., Hender, T.C, Carreras, B*et al.*, Phys. Fluids **30**, 1756 (1987)
[13] Hastie, R. J., and Hender,T.C., Nucl. Fusion **28**, 586 (1988)
[14] Waelbroeck, F., and Hazeltine, R., Phys. Fluids **31**, 1217 (1988)
[15] Bonfiglio, D., Cappello, S., and Escande, D. F., Phys. Rev. Lett. **94** 145001 (2005)
[16] Denton, R. E., Drake, J. F., and Kleva, R. G., Phys. Fluids **30** 1448 (1987)
[17] Jardin, S.C., Ferraro, N., Breslau, J., and Chen, J., Comput. Sci. & Disc., **5**, 014002 (2012)
[18] Halpern, F. D., Leblond, D., Lutjens, H. *et al.*, Plasma Phys. and Control. Fusion **53**, 015011 (2011)
[19] Breslau, J. A., Sovinec, C. R., and Jardin, S.C., Comm. in Comput. Phys. **4**, 647-658 (2008)
[20] Shen, W., Fu,G., Tobias,B. *et al.*, Phys. Plasmas **22**, 042510 (2015)
[21] Cappello, S.,Bonfiglio, D., and Escande, D.F., Phys. Plasmas **13**, 056102 (2006)
[22] Callen, J. D. , Cole, A. J., and Hegna, C. C., Phys. Plasmas **16**, 082504 (2009)
[23] Cooper, W. A., Chapman, I., Schmitz, O. *et al.*, Nucl. Fusion **53**, 073021 (2013)
[24] Casper, T. A., Jayakumar, R. J., Allen, S. L. *et al.* Nucl. Fusion **47**, 825-832 (2007)
[25] Chu, M. S., Brennan, D. P., Chan, V. S. *et al.* Nucl. Fusion **47**, 434-442 (2007)
[26] Garcia, J. and Giruzzi, G., Phys. Rev. Lett., **104**, 205003 (2010)
[27] Wolf, R., Gruber, O., Maraschek, M., *et al.* Plasma Phys. Control. Fusion **41** B93 (1999)
[28] Günter, S., Giruzzi, G., Gude, A. *et al.* Plasma Phys. Control. Fusion **41** B231 (1999)
[29] Wade, M. R., Luce, T. C., Jayakumar, R. J., *et al.* Nucl. Fusion **45**, 407 (2005)